Article
Vol. 26, No. 4, p. 455–467, August 2022
https://doi.org/10.1007/s12303-022-0003-4
pISSN 1226-4806 eISSN 1598-7477
Geosciences Journal GJ

Spatial variations of authigenic beryllium isotopes in surface sediments of the Antarctic oceans: a proxy for sea ice dynamics and sedimentary environments

Hyun Hee Rhee[1], Yeong Bae Seong[2]*, Min Kyung Lee[1], Ara Jeong[3], Chinmay Dash[2], Jae Il Lee[1], Kyu-Cheul Yoo[1], and Byung Yong Yu[4]

[1]Division of Glacial Environment Research, Korea Polar Research Institute, Incheon 21990, Republic of Korea
[2]Department of Geography Education, Korea University, Seoul 02841, Republic of Korea
[3]Department of Civil Engineering and Environmental Sciences, Korea Military Academy, Seoul 01805, Republic of Korea
[4]AMS Laboratory, Korea Institute of Science and Technology, Seoul 02792, Republic of Korea

ABSTRACT: This study documents spatial variations in authigenic ^{9}Be and ^{10}Be concentrations and ^{10}Be/^{9}Be ratios in different glacial settings in the Weddell and Ross seas, Antarctica. Weddell Sea surface sediments have the lowest ^{10}Be and highest ^{9}Be concentrations, and most depleted ^{10}Be/^{9}Be ratios, as compared with other regions, indicating ^{9}Be enrichment from the recently collapsed Larsen Ice Shelf (LIS) B and reduction of ^{10}Be supply due to blockage by the un-deglaciated LIS C. Local ^{10}Be deposition varies across the open marine Ross Sea, which is more affected by seasonal sea ice persistence than ocean currents. Higher ^{10}Be/^{9}Be ratios in the western Ross Sea and higher ^{10}Be concentrations in the eastern Ross Sea correlate with higher sea ice concentrations and changes, and vice versa in the central Ross Sea. The higher sea ice concentration not only blocks atmospheric ^{10}Be and dust deposition during the frozen season, but increases the dust flux and supply of Be isotopes during the sea ice melting season. Thus, the spatial distribution of Be isotopes in surface sediments of the Antarctic oceans can be used as a proxy for sea ice dynamics and sedimentary environments.

Key words: Antarctica, cosmogenic ^{10}Be, sea ice, oceanic sedimentation, local contamination offset

Manuscript received July 18, 2021; Manuscript accepted March 29, 2022

1. INTRODUCTION

The meteoric ^{10}Be produced in the upper atmosphere by cosmogenic spallation reactions becomes attached to dust and aerosols, and is deposited in sediments via dry and wet precipitation (Thor and Zutschi, 1958; Beer et al., 2012). The stable isotope ^{9}Be is transported to the oceans by riverine or glacial processes after weathering of Be-bearing minerals, and its spatial distribution varies with proximity to terrestrial sources (Bourles et al., 1989). Before being deposited on the ocean floor, Be isotopes become attached to particles or dissolved in seawater (authigenic) and are mixed in the ocean for ~1000 yr, depending on the site-specific conditions. Beryllium isotopes can trace local dust inputs, sediment pathways, and regional changes in water fluxes to the oceans (Brown et al., 1992a, 1992b). However, in ice-covered oceans, glacial advances or sea ice can block authigenic ^{10}Be precipitation onto the ocean floor, while the ^{9}Be supply continues from terrestrial sources via ocean currents. The ^{10}Be concentration of oceanic sediments increases abruptly in open marine conditions and vice versa (Scherer et al., 1998). ^{10}Be/^{9}Be record of marine sediments has been a faithful proxy to study deep marine circulation patterns (von Blanckenburg et al., 1996) and continental sedimentation to ocean basins (Willenbring and von Blanckenburg, 2010; von Blanckenburg and Bouchez, 2014; von Blanckenburg et al., 2015), as the ratio can circumvent the issues relating to grain size dependency and retention behavior. Be isotopes are subject to reworking but have different pathways than other cosmogenic radioisotopes (e.g., ^{14}C) (Sjunneskog et al., 2007), and hence can compensate for uncertainties associated with chronology and can illustrate changes in earth surface processes. Despite

***Corresponding author:**
Yeong Bae Seong
Department of Geography Education, Korea University, 145 Anam-ro, Seongbuk-gu, Seoul 02841, Republic of Korea
Tel: +82-2-3290-2367, E-mail: ybseong@korea.ac.kr

several advantages over traditional isotopes, the present understanding of the of Be isotope variability in different environmental settings has remained unclear. Moreover, in dynamic glacio-marine environments, like Antarctica, the complex characteristics of glacial and glacio-marine sediments do not offer easily interpretable environmental or chronological signals (Sjunneskog et al., 2007).

Previous studies on sediment records of Antarctic oceans using Be isotopes have revealed several glacial–interglacial transitions (Scherer et al., 1998; Sjunneskog et al., 2007; Yokoyama et al., 2016). These studies focused mostly on the transitions from sub-glacial or sub-ice shelf settings to open marine conditions, particularly for the most recent glacial and current interglacial periods. However, none of these studies have documented the spatial variability of meteoric ^{10}Be deposition. The hypothetical calculated ^{10}Be concentration is uniform for the Ross Sea (~9 × 10^7 atoms/g; Field et al., 2006; Heikkilä, 2007; Willenbring and von Blanckenburg, 2010), but reported ^{10}Be concentration records for the central and eastern Ross Sea have local offsets that are two orders of magnitude higher than these calculations (Sjunneskog et al., 2007; Yokoyama et al., 2016). Lower ^{10}Be concentrations characterize the area near the edge of the Ross Ice Shelf (RIS) as the sea ice blocks meteoric fallout. Other studies of Ross Sea sediments have also identified a local contamination offset (LCO) of old carbon, iron, and diatoms supplied via different atmospheric and oceanic pathways (Cunningham and Leventer, 1998; Wang et al., 2014; McGillicuddy Jr. et al., 2015; Prothro et al., 2020).

The LCO of old carbon (i.e., ^{14}C-depleted carbon) transported by ocean currents has been observed in surface sediments of the Ross Sea (Hillenbrand et al., 2010; Prothro et al., 2020), implying that ^{14}C ages in this region need to be corrected for the LCO, as well as the reservoir effect. McGillicuddy Jr. et al. (2015) modeled the iron supply to the Ross Sea via intrusion of circumpolar deep water and melting of sea and glacial ice, in order to identify the major productivity control on phytoplankton blooms in Antarctica. This showed that the major productivity control was melting of sea ice rather than other factors. Modeling of the iron supply from dust also confirmed the effects of sea ice, which limits the iron supply from dust in the southwestern Ross Sea (Wang et al., 2014). The variations in the spatial distribution of these elemental and isotopic proxies in the Antarctic sediments can be used to trace ^{10}Be pathways, especially in relation to the sea and glacial ice coverage.

The LCO of Be isotopes reflects a deviation from the estimated ^{10}Be flux or enhanced ^{9}Be flux due to proximity to glacial sources, which are largely the result of local sea ice and changes in exposure to atmospheric fluxes due to changes in the cryosphere. The sea ice persistence on the Arctic Ocean not only dominated the ^{10}Be fallout, but also transported it to the North Atlantic during the past 12.3 Ma (Eisenhauer et al., 1994; Frank et al., 2008). In the Southern Ocean, the export of ^{10}Be from the ice covered areas around the Antarctic margin likely resulted in high ^{10}Be deposition rates in the Antarctic Circumpolar Current system, in particular during the glacial stages of the Late Quaternary (Kumar et al., 1995; Frank et al., 2000). The settling and scavenging rate in the water column can cause the LCO, as well as blocking of the atmospheric ^{10}Be supply by the presence of sea ice, partial dissolution of the detrital terrigenous particles, reworking or redistribution of the marine sediments (Frank et al., 1995; von Blanckenburg et al., 1996; Frank et al., 2002; Sjunneskog et al., 2007; Frank et al., 2009; von Blanckenburg and Bouchez, 2014). Combined ^{10}Be/^{9}Be ratios and ^{10}Be concentrations can be used to correct for the offsets caused by different sedimentation rates, particle sizes, sediment storage, and water mass mixing (Eisenhauer et al., 1994; Simon et al., 2016; Valletta et al., 2018).

This study investigates authigenic ^{10}Be and ^{9}Be concentrations and ^{10}Be/^{9}Be ratios of surface marine sediments in various glacial settings in Antarctica: non-glaciated areas (Southern Ocean; SO), post-LGM-deglaciated areas (RIS; 20–10 ka; Lowry et al., 2020), recently deglaciated areas (Larsen Ice Shelf [LIS] B; AD 2002; Shepherd et al., 2003), and non-deglaciated areas (LIS C; AD 2017). We also examined how the LCO of authigenic ^{10}Be and the ^{10}Be/^{9}Be ratio vary across the open marine areas of the Ross Sea by comparing surface isotope data with sea ice persistence or extent. Documenting the LCO of ^{10}Be on the ocean floor would improve its applicability to sedimentary and paleoenvironmental studies, such as phytoplankton blooms, in Antarctica.

2. STUDY AREA

The Ross and Weddell seas have the largest ice shelves in the world (Fig. 1a). Paleoenvironmental information is recorded in sediments in this region, which were influenced by ice advances and retreats during glacial–interglacial periods. The RIS drains both the West and East Antarctic ice sheets (WAIS and EAIS) into the Ross Sea and has maintained its present open ocean state since ca. 10 ka (Lowry et al., 2020). Local outlet glaciers that drain Marie Byrd Land and Victoria Land also flow into the Ross Sea. The Weddell Sea also contains several ice shelves fed by both the WAIS-EAIS (Ronne-Filchner Ice Shelf) and the Antarctic Peninsula (LIS A, B, and C), within the largest embayment of Antarctica.

We collected sediment cores on several R/V Araon cruises by the Korea Polar Research Institute (KOPRI) in 2013 (Weddell Sea), 2015 (Ross Sea), and 2019 (Ross Sea). LIS B and C drain Antarctic Peninsula glaciers into the Weddell Sea, and recently

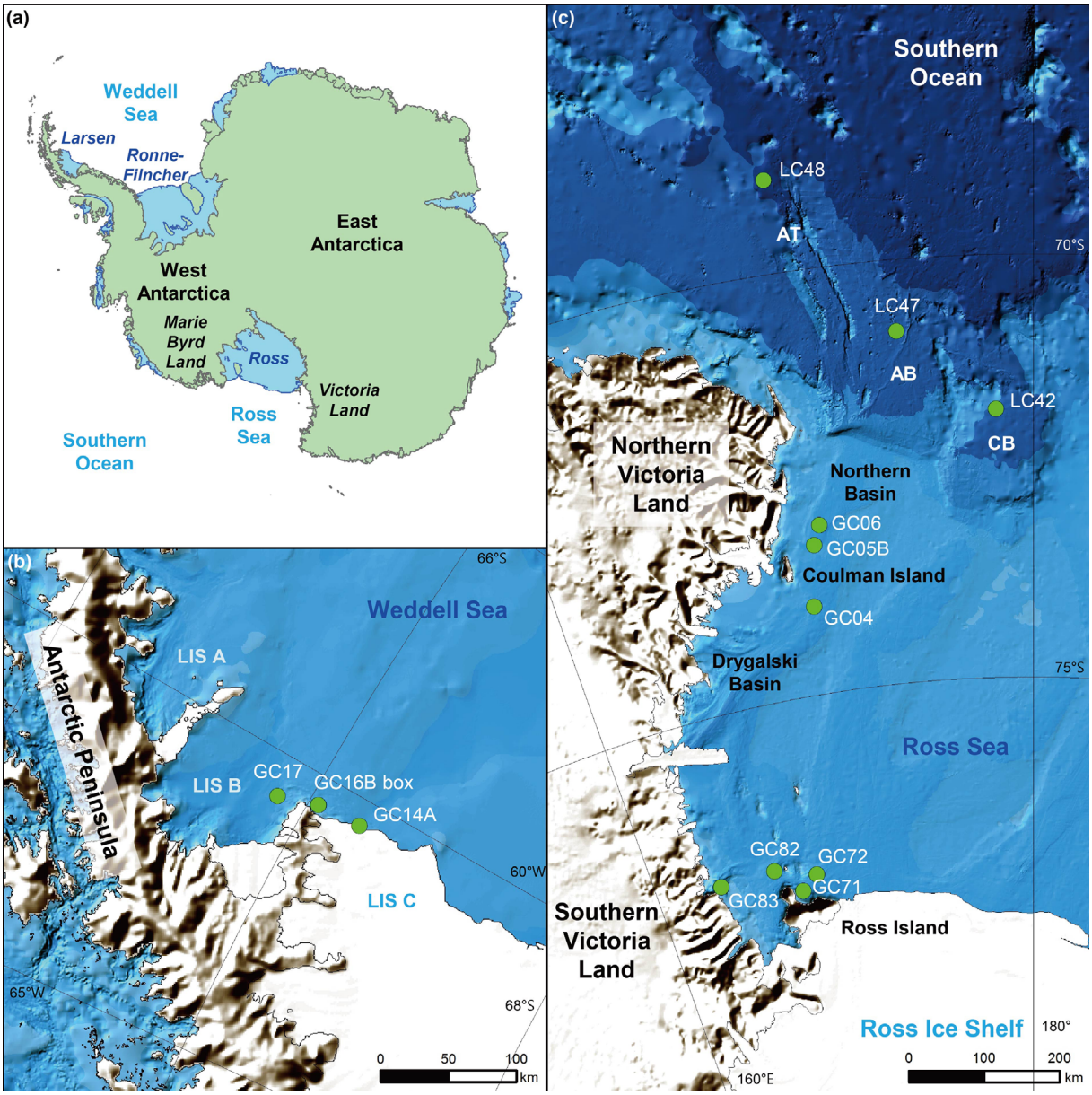

Fig. 1. (a) Map of Antarctica and its ice shelves. (b) Topographic map of the Antarctic Peninsula and LIS A, B, and C. Green circles are the locations of the sediment cores. (c) Topographic map of the western Ross Sea and Southern Ocean (AT = Adare Trough; AB = Adare Basin; CB = Central Basin).

collapsed in 2002 and 2017, respectively (Fig. 1b; Shepherd et al., 2003). We obtained sediment cores from the collapsed area of LIS B (GC17) and the sub-ice shelf area of LIS C (GC16B box and 14A) during the 2013 cruise (Jeong et al., 2018; Jung et al., 2019).

The RIS front occurs near Ross Island (RI), and we collected four sediment cores around RI and the Mackay outlet glacier (GC71, 72, 82, and 83; Fig. 1c). Another three sediment cores were collected from the Northern Drygalski Trough, which is located offshore of the RIS near Coulman Island (CI; GC04, 05B, and 06). This location was affected by the LGM advance of the RIS and outlet glaciers (Tucker-Aviator) draining Northern Victoria Land, and transitioned to an open ocean state earlier than RI. The other three cores were collected much further offshore of the RIS, on the continental slope and rise of the SO (LC42 in the Central Basin; LC47 in the Adare Basin; LC48 in the Adare Trough; Fig. 1c).

3. METHODS

3.1. Beryllium Isotope Analysis

Approximately 2 g samples were collected from the top surfaces of the cores (0–1 cm). The samples were dried and disintegrated in a ceramic mortar to remove grains larger than

https://doi.org/10.1007/s12303-022-0003-4

fine sand, which can cause a grain size dependency error. Only clay and fine silt particles were combusted at 450 °C in the furnace to remove organic materials by oxidation. We used a hybrid method for extracting authigenic Be and preparing samples for ^{9}Be concentration measurements by inductively coupled plasma mass spectrometry (ICP-MS) and ^{10}Be/^{9}Be ratios by accelerator mass spectrometry (AMS) installed at Korea Institute of Science and Technology, Seoul (Jeong et al., 2018).

We agitated ~1 g of each sample for 6 h in low-concentration acetic acid (25%) and diluted hydroxylamine hydrochloride (0.04 M) to extract authigenic Be (Bourles et al., 1989). Aliquots were sub-sampled for measurements of the ^{9}Be concentrations in the Korea Basic Science Institute (KBSI), Seoul, Korea. We mixed ~0.4 g of ^{9}Be carrier (~1000 ppm ^{9}Be with a low ^{10}Be content in concentrated HNO_3) into the residual samples for the AMS measurements. Samples were dried down in Pt crucibles to be mixed with KHF_2 and Na_2SO_4 (Stone, 1998). These reagents react with Be to make it water-soluble, whereas other cations are insoluble, while heating the crucible. We agitated the fluoride cake in Milli-Q water to collect the dissolved Be and precipitated and removed the K with $HClO_4$. Beryllium was recovered in HNO_3 and then precipitated as BeOH in a NH_4OH solution. The samples were then calcinated to BeO and mixed with Nb powder for the AMS measurements.

3.2. Spatial Correlation of Be Isotopes

We compared the Be concentrations and ^{10}Be/^{9}Be ratios to determine the LCO for Be in the Ross Sea. Summer sea ice concentrations were compared with Be isotopes using correlation analysis. The R^2 values of linear regressions and Pearson's correlation coefficients were used to quantify the correlations. Given that both sea ice concentration and persistence might be important, we also applied kernel interpolation to the data to compare it with the monthly sea ice extent and persistence in Antarctica (Fetterer et al., 2017). The kernel interpolation is a version of the inverse distance weighting method that combines locally fitted piecewise linear functions, which is based on the Delaunay triangulation (Mühlenstädt and Kuhnt, 2011). It is an alternative method to the Kriging technique, with minimal roughness properties in two dimensions, which is advantageous for a small number of samples with non-stationary behavior.

4. RESULTS

4.1. Beryllium Isotope Variations in Different Glacial Settings

The authigenic ^{9}Be concentration was calculated from the ICP-MS results, and then the authigenic ^{10}Be concentration was calculated using the ^{10}Be/^{9}Be ratio obtained from the AMS measurements (Table 1). We measured three standard samples (07KNSTD 5-1, 5-2, and 5-3; Nishiizumi et al., 2007) during each AMS measurement (n = 15). The correlations between the reference and measured standard values showed a high correlation with $R^2 > 0.999$. We normalized all the data with respect to the 07KNSTD sample 5-1 (2.709×10^{-11}), and deducted the ^{10}Be blank based on fourteen full procedural blanks (0.52–5.29×10^{-14} in ^{10}Be/^{9}Be (Tables 1 and 2).

The recently uncovered Weddell Sea LIS B (GC17) and C (GC16B box and 14A) cores have higher ^{9}Be concentrations than the other regions ($2.89 \pm 0.72 \times 10^{16}$ atoms/g), but the lowest ^{10}Be concentrations ($2.72 \pm 2.31 \times 10^{8}$ atoms/g) and authigenic ^{10}Be/^{9}Be ratios ($0.47 \pm 0.29 \times 10^{-8}$) (Fig. 2). Around the LIS, the earlier collapsed LIS B has higher concentrations of both Be isotopes than the later LIS C. ^{10}Be/^{9}Be ratios are also higher for LIS B, but are still much lower than the open marine regions.

The SO cores (LC42, 47, and 48), which are farthest offshore and have not been covered by the RIS, exhibit variable results for both Be isotope concentrations. LC42 has the lowest ^{9}Be and ^{10}Be concentrations, similar to those of CI. The highest ^{10}Be concentration occurs at LC47, which is an order of magnitude greater than the other cores, and a similar pattern was observed for the ^{9}Be concentrations. The extreme and mean ^{9}Be concentration ($2.03 \pm 0.82 \times 10^{16}$ atoms/g) of SO cores is lower than the Weddell Sea cores, but higher than the other embayment regions. The SO cores have the highest ^{10}Be concentration ($9.22 \pm 5.47 \times 10^{8}$ atoms/g) and authigenic ^{10}Be/^{9}Be ratio ($4.36 \pm 0.97 \times 10^{-8}$).

The CI cores (GC04, 05B, and 06) have the lowest ^{9}Be ($1.10 \pm 0.10 \times 10^{16}$ atoms/g) and ^{10}Be ($4.04 \pm 0.95 \times 10^{8}$ atoms/g) concentrations of the Ross Sea cores. Their ^{10}Be concentrations are higher than the Weddell Sea cores where recent ice shelf collapse has occurred, while the ^{9}Be concentrations are much lower with little spatial variability. Authigenic ^{10}Be/^{9}Be ratios of the CI cores are lower than the offshore regions (i.e., SO) and higher than onshore areas (e.g., RI) ($3.69 \pm 0.70 \times 10^{-8}$).

The RI cores (GC71, 72, 82, and 83) have lower ^{9}Be concentrations ($1.86 \pm 0.16 \times 10^{16}$ atoms/g) than most offshore SO cores. Their ^{10}Be concentrations ($6.09 \pm 0.31 \times 10^{8}$ atoms/g) are also lower than the offshore cores, but higher than the CI cores. Both Be isotopes show a lower statistical variation of their concentrations than in the other regions and their ^{10}Be/^{9}Be ratios show the lowest values and accordingly smallest statistical variability ($3.28 \pm 0.25 \times 10^{-8}$). Across the western Ross Sea (WRS), ^{9}Be concentrations are higher near the edge of the RIS (RI cores) and tend to decrease further offshore (CI cores), similar to the ^{10}Be concentrations. In contrast, ^{10}Be/^{9}Be ratios across the WRS

Table 1. Authigenic ^{10}Be and ^{9}Be data for surface sediments from Antarctica

Core code	Lat [S]	Lon [+, E] [, W]	Sample mass [g]	Carrier conc. [ppm][(a)]	Carrier mass [g]	^{9}Be counts in sample [1E16 atoms/g][(b)]	AMS $^{10}Be/^{9}Be$ ratio [1E−11][(c), (d)]	Blank level [1E−14][(d), (e)]	^{10}Be counts in sample [1E8 atoms/g][(d)]	Authigenic $^{10}Be/^{9}Be$ ratio [1E−8][(d), (f)]
Weddell Sea										
EAP13-GC17	65°48.1656	−60°39.4296	0.5030	1093.34	0.4110	3.583 ± 0.174	1.112 ± 0.012	5.294 ± 0.607	5.992 ± 0.065	0.839 ± 0.009
EAP13-GC16B	66°03.8983	−60°27.4921	0.5069	1018.06	0.3904	2.085 ± 0.064	0.584 ± 0.006	5.294 ± 0.608	2.734 ± 0.028	0.408 ± 0.004
EAP13-GC14A	66°22.2306	−60°25.2807	0.9421	1047.80	0.4059	2.505 ± 0.049	0.409 ± 0.007	0.832 ± 0.258	1.268 ± 0.025	0.506 ± 0.010
						2.898 ± 0.720			***2.727 ± 2.314***	***0.472 ± 0.290***
Southern Ocean/Ross Sea										
Adare Trough										
RS15-LC48	68°53.9289	171°09.8914	1.0131	1053.60	0.4046	2.126 ± 0.005	2.645 ± 0.016	0.529 ± 0.243	7.537 ± 0.047	3.545 ± 0.022
Adare Basin										
RS15-LC47	70°50.7003	175°04.1603	1.0010	1053.60	0.4050	2.816 ± 0.011	5.379 ± 0.027	0.529 ± 0.243	15.350 ± 0.078	5.450 ± 0.071
Central Basin										
RS15-LC42	71°49.3969	178°34.7602	0.9805	1053.60	0.3802	1.167 ± 0.005	1.706 ± 0.031	0.825 ± 0.249	4.792 ± 0.003	4.105 ± 0.017
						2.036 ± 0.828			***9.226 ± 5.478***	***4.367 ± 0.979***
Ross Sea										
Coulman Island										
RS19-GC06	73°00.8030	171°18.7757	1.0044	983.56	0.3738	0.987 ± 0.021	1.272 ± 0.009	3.581 ± 0.460	3.105 ± 0.038	3.161 ± 0.066
RS19-GC05B	73°14.2519	170°58.6333	1.0229	1047.80	0.3945	1.196 ± 0.034	1.494 ± 0.013	3.581 ± 0.460	4.028 ± 0.053	3.445 ± 0.098
RS19-GC04	73°57.4102	170°34.0365	1.0213	1047.80	0.3805	1.140 ± 0.027	1.925 ± 0.016	3.581 ± 0.460	5.014 ± 0.065	4.490 ± 0.106
						1.108 ± 0.108			***4.049 ± 0.955***	***3.699 ± 0.700***
Ross Island										
RS15-GC82	76°56.6123	166°17.1496	1.0324	1053.60	0.4005	1.880 ± 0.009	2.111 ± 0.021	0.529 ± 0.243	5.954 ± 0.060	3.166 ± 0.034
RS15-GC83	76°57.7681	166°22.9994	1.0124	1053.60	0.4220	2.085 ± 0.012	2.116 ± 0.017	0.529 ± 0.243	6.289 ± 0.049	3.016 ± 0.046
RS15-GC71	77°05.1755	168°26.2231	1.0019	1053.60	0.4064	1.700 ± 0.007	2.001 ± 0.015	0.529 ± 0.243	5.728 ± 0.042	3.370 ± 0.027
RS15-GC72	77°14.7225	167°33.7824	1.0274	1053.60	0.4157	1.782 ± 0.008	2.190 ± 0.017	0.529 ± 0.243	6.413 ± 0.049	3.599 ± 0.036
						1.862 ± 0.166			***6.096 ± 0.313***	***3.287 ± 0.253***
Yokoyama et al. (2016)[(g)]										
GC1604	74.55°	168°							11	
TC31	75.17°	178.548°							17	
TC04	78.15°	−168.58°							10	
TC07	77.23°	−169.419°							15	
KC11	76.31°	−169.659°							35	
Sjunneskog et al. (2007)[(g)]										
TC18						17.347			5.1	0.294
TC16						10.256			12.	1.170
TC11						9.434			2.5	0.265
PC31						9.467			16	1.690

[(a)]Concentration of ^{9}Be dissolved in HNO_3 solution.
[(b)]^{9}Be concentration was calculated from the Inductively Coupled Plasma Mass Spectrometry (ICP-MS) measurement results.
[(c)]07KNSTD 5-1 reference samples (2.709E−11) were used for normalization of the AMS results (Nishiizumi et al., 2007).
[(d)]Uncertainties were calculated at the 1σ confidence level.
[(e)]Mean values of process blank samples were used for correction of background.
[(f)]Ratios of authigenic $^{10}Be/^{9}Be$ were calculated from the concentrations of each isotope.
[(g)]Reffered.

Table 2. Chemical process blanks

Blank code	Carrier conc. [ppm]	Carrier mass [g]	AMS $^{10}Be/^{9}Be$ Ratio [1E−14]	^{10}Be counts in blank [1E5 atoms/g]
kuba006	1018.1	0.3936	3.573 ± 0.299	17.571 ± 1.475
kuba007	1018.1	0.3929	2.198 ± 0.361	10.789 ± 1.774
KUBkM1601	1053.6	0.3733	0.474 ± 0.125	2.170 ± 0.654
KUBeBkM1603	1053.6	0.3924	0.208 ± 0.150	1.162 ± 0.503
KUBeBkM1604	1053.6	0.3980	0.552 ± 0.548	3.127 ± 1.106
KUBeBkM1605	1053.6	0.3958	0.135 ± 0.128	0.763 ± 0.539
KUBeBkM1606	1053.6	0.4007	0.152 ± 0.024	0.866 ± 0.567
KUBkM1903	1047.8	0.4027	0.495 ± 0.122	2.705 ± 0.999
KUBkM1904	1047.8	0.4083	0.365 ± 0.122	2.021 ± 0.464
KUBkM2001	1047.8	0.3903	0.847 ± 0.076	4.373 ± 0.798
KUBkM2002	1047.8	0.3878	0.616 ± 0.027	3.158 ± 0.731
KUBkM2003	983.6	0.3926	2.301 ± 0.539	11.217 ± 1.165
KUBkM2004	983.6	0.3912	1.015 ± 0.232	4.928 ± 1.067
KUBkM2005	983.6	0.4845	4.710 ± 1.028	28.330 ± 2.782

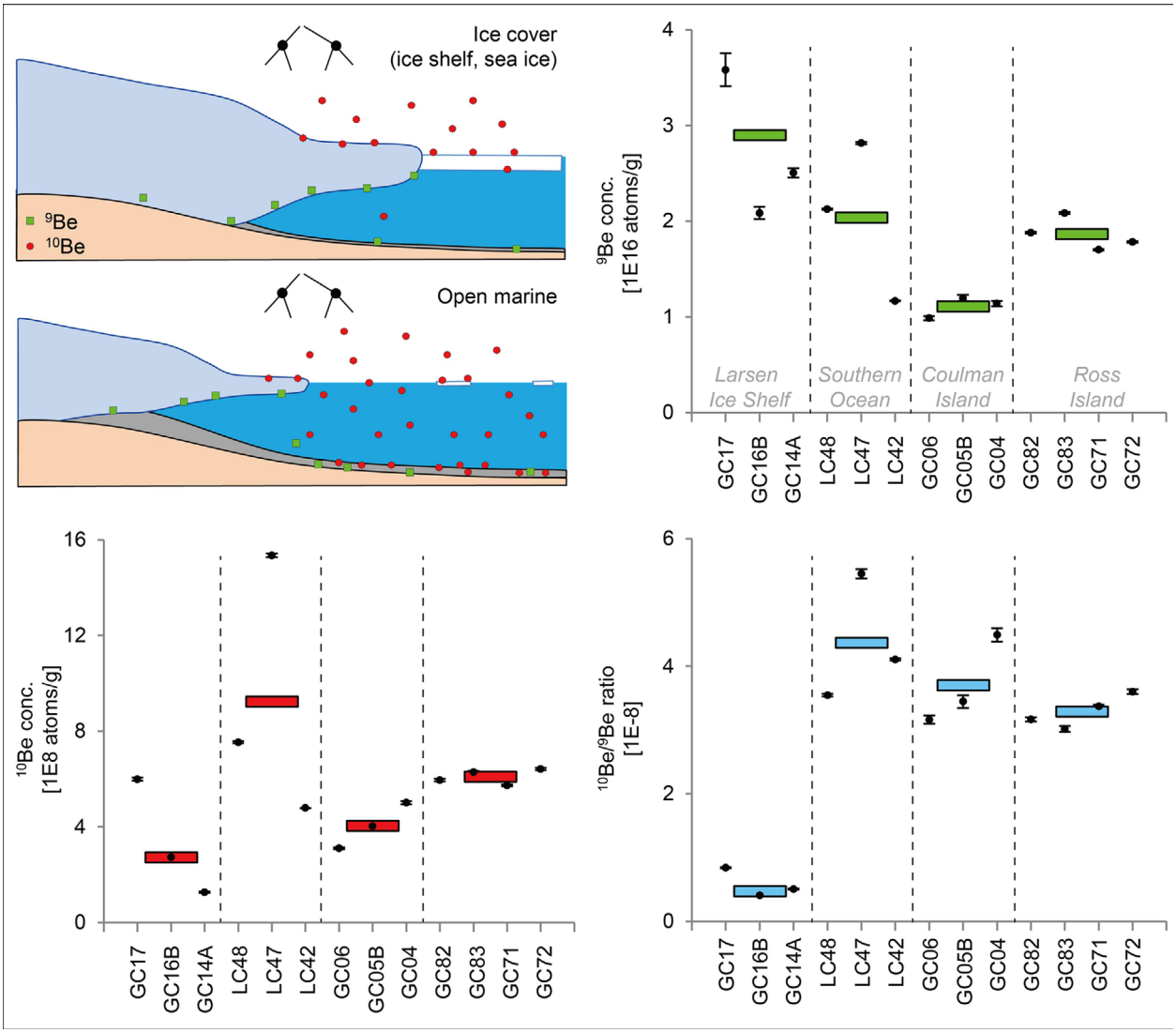

Fig. 2. Conceptual source models of the terrestrial ^{9}Be (green squares) and authigenic ^{10}Be fluxes (red circles), and the results of the authigenic ^{10}Be, ^{9}Be, and $^{10}Be/^{9}Be$ analyses. Colored boxes are the mean values of each region.

appear to be higher on the outer shelf than in the inner Ross embayment.

4.2. Beryllium Isotope Variations in Open Marine Conditions (Local Contamination Offsets)

Local Contamination Offsets (LCO) of Be isotopes appear among the open marine conditions on the Ross Sea. WRS cores (RI and CI) have low ^{9}Be and ^{10}Be concentrations as compared with the central (CRS) and eastern Ross Sea (ERS; Figs. 3 and 4). In contrast, ^{10}Be/^{9}Be ratios across the WRS are higher than those in the CRS. According to the latitude or distance from the edge of the RIS, ^{9}Be concentrations in both the WRS and CRS are higher near the edge than further north, especially in the CRS. ^{10}Be also appears to decrease moving toward the onshore WRS, whereas it tends to increase across the CRS and ERS. ^{10}Be concentrations along the ERS not only increase to the highest value near its edge, but also show the largest gap between the onshore and offshore regions.

Both the ^{10}Be concentrations and ^{10}Be/^{9}Be ratios were compared with local summer (DJF) mean sea ice concentrations by simple linear fitting and a Pearson's correlation analysis (Fig. 5). Surface ^{10}Be concentrations in the Ross Sea generally have a positive correlation with the sea ice concentration ($R^2 = 0.06$ and $\rho = 0.26$), except in the WRS ($R^2 = 0.67$ and $\rho = -0.82$). The correlation coefficients for the CRS and ERS are higher as compared with all the data ($R^2 = 0.11$ and $\rho = 0.34$, and $R^2 = 0.97$ and $\rho = 0.98$, respectively). ^{10}Be/^{9}Be ratios in the WRS and CRS also exhibit a

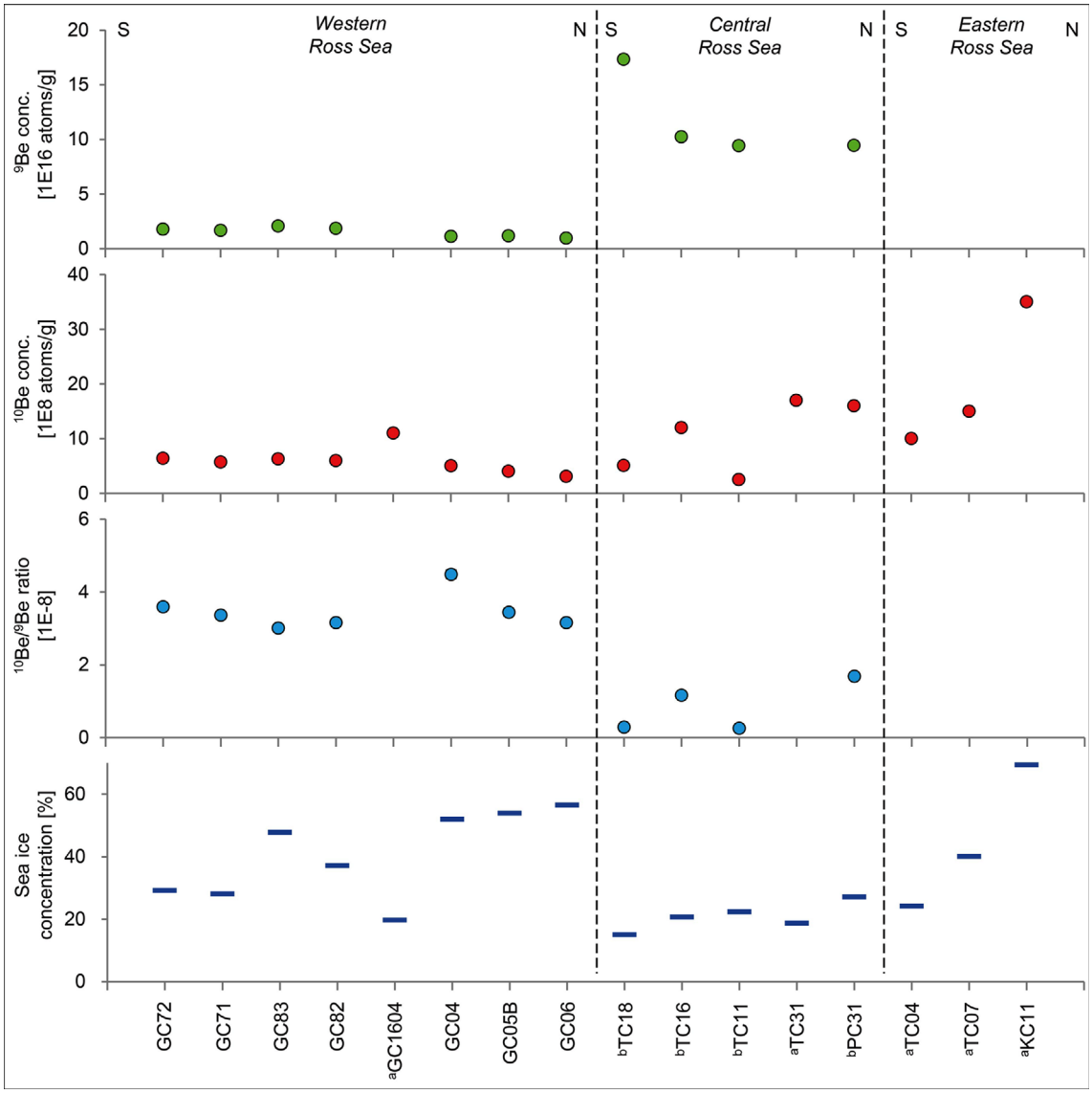

Fig. 3. Surface concentrations of ^{9}Be and ^{10}Be, and ^{10}Be/^{9}Be ratios on the Ross Sea seafloor from south (S) to north (N) along each sector (a: Yokoyama et al., 2016; b: Sjunneskog et al., 2007; this study). The blue bars are the mean sea ice concentration during the Austral summer at each core location.

https://doi.org/10.1007/s12303-022-0003-4

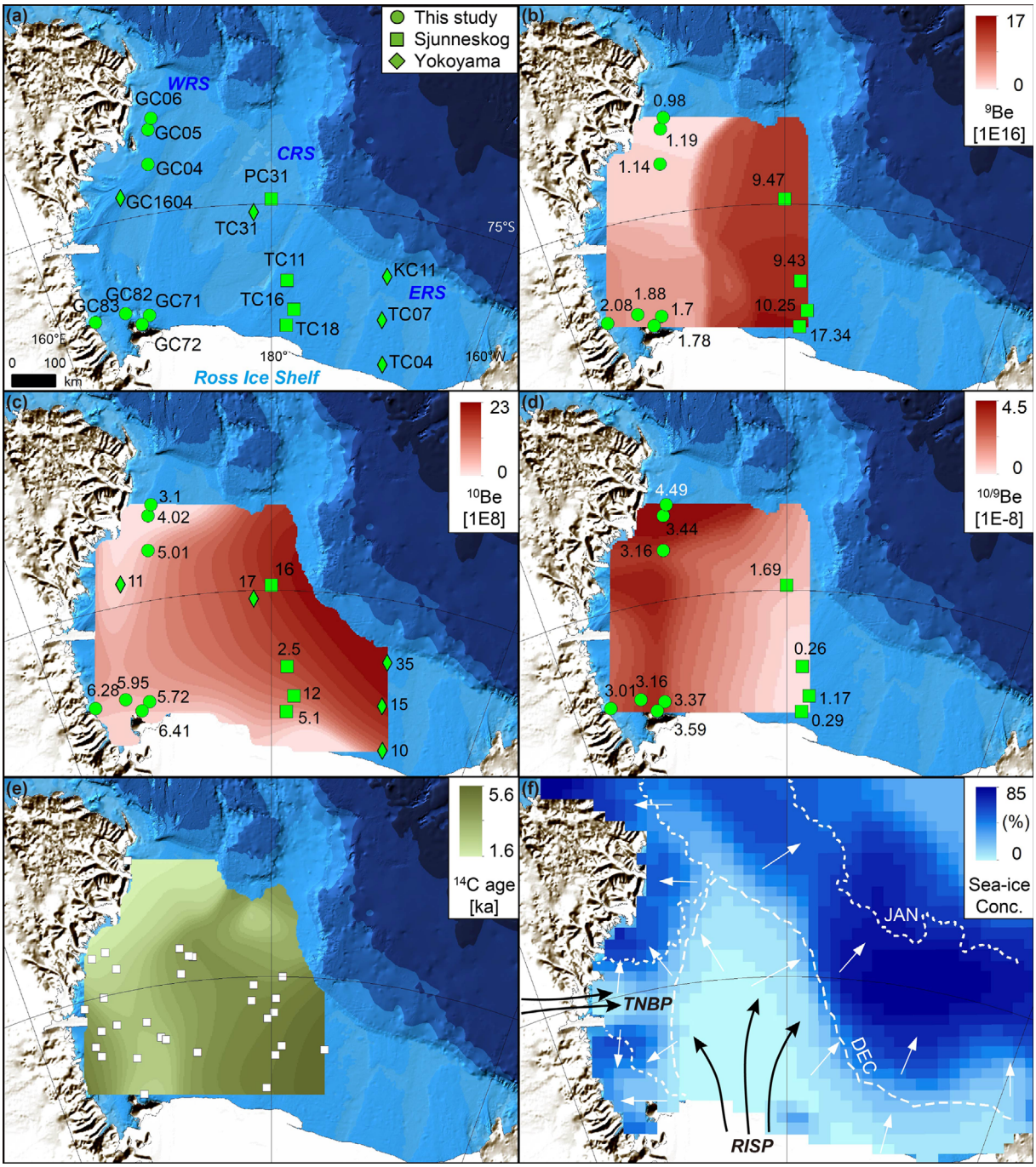

Fig. 4. (a) Location of sediment cores in the Ross Sea (Sjunneskog et al., 2007; Yokoyama et al., 2016; this study). (b–d) Surface ^{9}Be and ^{10}Be concentrations (atoms/g) and ^{10}Be/^{9}Be ratios and their kernel interpolated results. (e) Kernel interpolated results of surface ^{14}C dating revealing the old carbon LCO (Prothro et al., 2020). (f) Sea ice concentration and extent during summer (Fetterer et al., 2017). Early opening of sea ice is mainly due to the katabatic wind (black arrow; TNBP = Terra Nova Bay Polynya; RISP = Ross Ice Shelf Polynya; Sedwick et al., 2011).

positive correlation with the sea ice concentration (R^2 = 0.57 and ρ = 0.75), but the WRS has a poor correlation. However, both the ^{10}Be concentrations and ^{10}Be/^{9}Be ratios along the WRS coast are relatively uniform, which accounts for the poor correlation (Fig. 5). The kernel interpolated graphical distributions show that Be deposition and sea ice variations differ between the WRS coast and the CRS and ERS regions (Fig. 4).

5. DISCUSSION

5.1. Spatial Variations of Be Isotopes in Different Glacial Settings

^{9}Be in the ocean is supplied by glacial and/or riverine sediments that are weathered from terrestrial rocks and, therefore, records

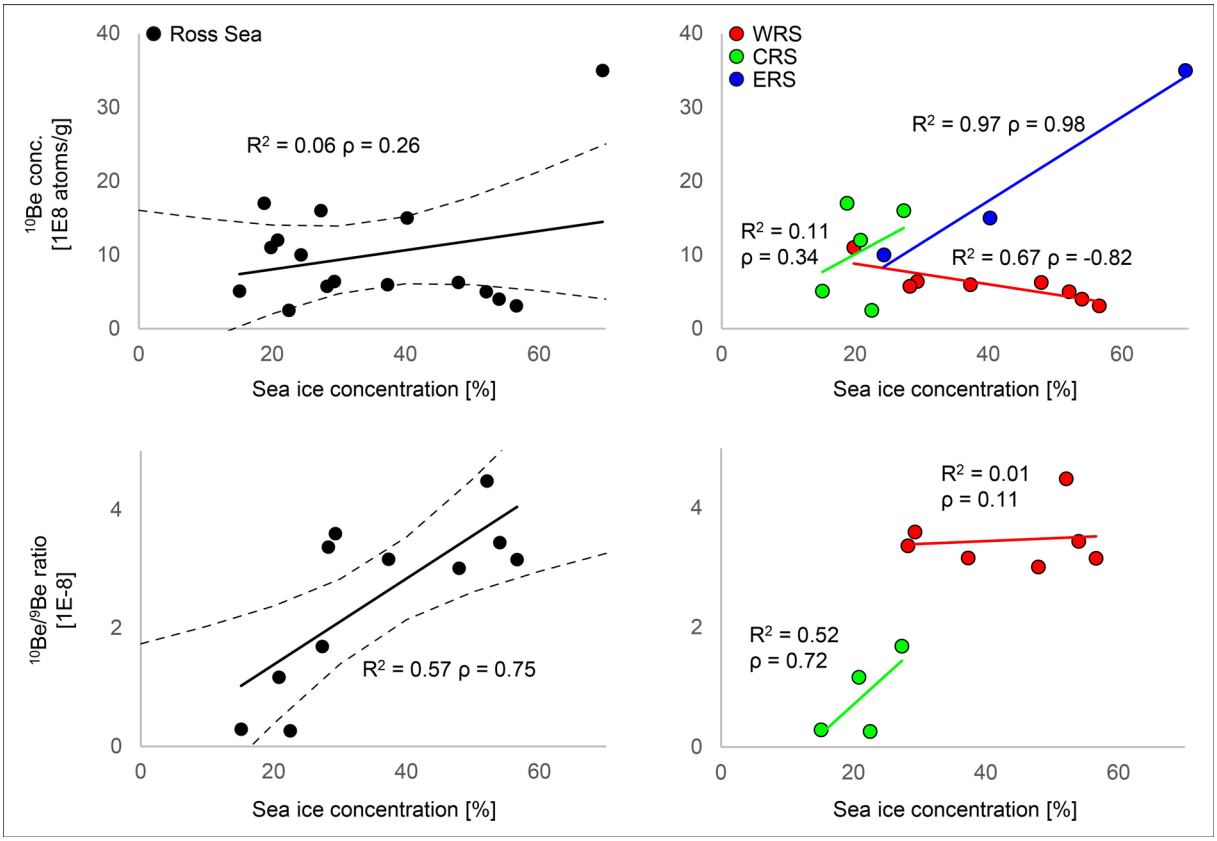

Fig. 5. Scatter plots, best-fit linear regressions, and R^2 and Pearson's r values (ρ) for the sea ice concentration versus the ^{10}Be concentration and ^{10}Be/^{9}Be ratios in the Ross Sea. Dashed lines represent 95% confidence limits of the linear fits. Different colored data reflect each sector of the Ross Sea (red = western; green = central; blue = eastern).

the proximity to glacial melt-water sources or the sediment sources and transport (i.e., ocean currents) to ocean basins (Bourles et al., 1989; Brown et al., 1992a, 1992b; Sjunneskog et al., 2007; Valletta et al., 2018). ^{10}Be in the ocean is supplied by wet precipitation or dust particles from the atmosphere. Ice coverage and ocean circulation can affect the depositional patterns of Be isotopes. We compared the ^{9}Be and ^{10}Be concentrations and ^{10}Be/^{9}Be ratios to examine the differences in the modern sedimentation environment in the Weddell Sea (recently collapsed or sub-ice shelf setting), SO (non-glaciated open marine setting), and Ross Sea (deglaciated open marine setting; Fig. 2).

In general, the surface marine sediments collected from the Weddell Sea have the lowest ^{10}Be and highest ^{9}Be concentrations as compared with the other regions (Fig. 2). This is because the ^{10}Be supply had been blocked by the LIS B until 2002 when it collapsed, or the ^{10}Be supply is still blocked by the LIS C. In contrast, ^{9}Be is supplied via sub-glacial melting under the sub-ice shelf, leading to abundant input of ^{9}Be in this region. Grain size data for Weddell Sea continental slope sediments also reveal that ice-rafted debris is the dominant component in these sediments (Diekmann and Kuhn, 1999), suggesting the higher inputs of ^{9}Be are due to sub-glacial melting and partial dissolution of ice-rafted materials. However, considerable variation in Be isotopes was observed between the LIS B and C, which reflect their different glacial settings—recently deglaciated (LIS B) and non-deglaciated (LIS C) (Fig. 2). The large input of sub-ice shelf-sourced ^{9}Be and restricted supply of authigenic ^{10}Be due to sea ice coverage results in extremely low ^{10}Be/^{9}Be ratios as compared with the other open marine settings.

Three cores from the SO yielded variable results (Fig. 2). Both ^{10}Be and ^{9}Be concentrations in the LC42 and LC48 cores have similar concentrations to the other open marine settings, while the LC47 core (Adare Basin) has significantly higher concentrations. ^{9}Be concentrations are higher than in the sub-ice shelf setting (LIS), even though LC47 is distant from glaciated regions and the continental area. Both high ^{10}Be and ^{9}Be concentrations imply that the Adare Basin is an ideal setting for the redistributed delivery of isotopes into the sediments. This is consistent with the high sedimentation rates in the Adare Basin during the late Pleistocene as compared with the other cores (Ohneiser et al., 2019). ^{10}Be/^{9}Be ratios are also highest of the studied cores, which reflect the limited influence of the Antarctic cryosphere.

The RI cores (GC71, 72, 82, and 83) have relatively uniform

 https://doi.org/10.1007/s12303-022-0003-4

^{10}Be and ^{9}Be concentrations, despite their different outlet glacial sources, ice flow lines, and topographic settings. This indicates there is a similar sedimentary environment around RI. The CI cores (GC04, 05B, and 06) also show little difference in ^{9}Be concentrations, although they were sampled along the northern Drygalski Trough with different outlet glacial sources (Figs. 1c and 2). However, ^{10}Be concentrations and ^{10}Be/^{9}Be ratios vary significantly along the Drygalski Trough. The uniform supply of terrestrial ^{9}Be suggests stable sedimentation is occurring below sea level, whereas there is a variable supply from the atmosphere (^{10}Be). This implies that local offset effects can occur, controlled by the surficial environment, such as sea ice coverage, rather than ocean circulation (Fig. 2).

Compared with the RI region, ^{9}Be concentrations are about half those on the CI seafloor. Given that both regions are located in front of outlet glaciers, the terrestrially sourced ^{9}Be may be being affected by lithological differences in the source area rather than by ocean circulation or continental proximity. In addition, the RI cores are located more proximal to the RIS than the CI cores, and the higher ^{9}Be flux might be due to its proximity to a larger glacial source. The LCO of authigenic ^{10}Be is marked within the CI region, and greater than that of the RI region.

^{10}Be concentrations in the post-LGM-deglaciated areas (RI and CI) are generally higher than in recently deglaciated (LIS B) and non-deglaciated areas (LIS C), but lower than in non-glaciated areas (SO) (Fig. 2). Different glacial settings cause variable ^{10}Be inputs due to the cryospheric effects, even though secondary scavenging, mixing, and reworking have occurred. However, ^{10}Be/^{9}Be ratios exhibit more consistent trends with different sedimentary environments or the secondary reworking than ^{10}Be concentrations. ^{10}Be/^{9}Be ratios are lowest in the LIS area and highest in the SO. In general, SO waters have a slightly higher ^{10}Be/^{9}Be ratio (10×10^{-8}) than global average deep-water ($\sim 8 \times 10^{-8}$; von Blanckenburg and Bouchez, 2014). However, the lower ratios ($3.5–5.4 \times 10^{-8}$) measured in this study are consistent with those ($0.5–5.0 \times 10^{-8}$) measured near the East Antarctic continental margin (Wilkes Land), which is affected by a higher terrigenous ^{9}Be input (Valletta et al., 2018). Lower ^{10}Be/^{9}Be ratios for the deglaciated areas (Ross Sea) and near the LIS also reflect glacial input and proximity to the continental region.

Our compiled ^{10}Be data from marine sediment cores across the Ross Sea are with lack of modern local sedimentation rate which can affect the dilution of ^{10}Be deposition. Some of the reasons why we cannot at present correlate our Be isotope data with sedimentation rate are: i) First of all there are no studies mentioning recent sedimentation rate in the Antarctic Oceans. All the studies concerning sedimentation are primarily based on provenance and how geomorphology controls sedimentation. ii) wherever sedimentation rates can be calculated, they are based on coarse chronological records. Hence obtaining a recent sedimentation rate would lead to significant errors. iii) Except for the dilution effect of sediments, partition coefficient and grain size also affect the concentration of ^{10}Be. Since our results on ^{10}Be are corroborating the ^{10}Be/^{9}Be, the particle size retention behaviour and dilution effect can be ignored. Hence any possible effect of sedimentation rate on Be isotope concentration can be analyzed only if modern sedimentation rates are obtained. Nevertheless, no significant fluctuation of dissolved Pb concentration in the lateral and vertical transect across the Ross Sea show that much more homogeneous or stable deposition of particles are proceeded through the water column than expected (Gerringa et al., 2020). ^{10}Be/^{9}Be data would compensate for the sedimentation rate correction, but additional sediment trap studies would develop our discussion in near future.

5.2. Surface Local Contamination Offsets of ^{10}Be in Open Marine Setting (Ross Sea)

Open marine regions are also affected by seasonal sea ice extent or persistence. Unlike an ice shelf, seasonal sea ice stores meteoric ^{10}Be fallout during the winter, ice-covered period, and then releases ^{10}Be if seasonal melting occurs. We compared our seafloor Be data for the WRS with the CRS, ERS, and sub-RIS (Sjunneskog et al., 2007; Yokoyama et al., 2016), which used the similar, conventional analytical method (Figs. 3 and 4a). Mean ^{10}Be concentrations in the WRS are 2–3 times lower than those in the CRS and ERS. ^{9}Be concentrations in the WRS are an order of magnitude lower than in the CRS, while the ^{10}Be/^{9}Be ratio in the WRS is ~4 times higher than that in the CRS.

^{10}Be concentrations in the open marine Ross Sea region are an order of magnitude higher than in the sub-RIS cores, which have the lowest ^{10}Be concentrations in the region. ^{10}Be/^{9}Be ratios are also lower in the sub-RIS cores, as compared with the Ross Sea, which reflects the ice shelf barrier to meteoric ^{10}Be deposition. In contrast, ^{9}Be concentrations tend to be higher near the RIS regions, and are even higher in the sub-RIS area. The sub-glacial-derived ^{9}Be is an order of magnitude higher in concentration than at the LIS (Fig. 2), which is related to the proximity to and scale of glacial activity.

The decrease in the ^{9}Be LCO along the CRS, from the edge to the outer area of the RIS, is due to a melt-water flux from the RIS (Figs. 3 and 4b). The WRS cores also have higher ^{9}Be concentrations near the RIS (i.e., RI cores) than in the open ocean regions (i.e., CI cores), which reflect the proximity to the melt-water flux from the RIS. However, the much lower ^{9}Be concentrations in the WRS as compared with the CRS is because the latter is affected by the proximal flux from Victoria Land outlet glaciers rather than the distal RIS. The ^{9}Be

concentrations in the WRS, where only local outlet glaciers occur, are lower than elsewhere in the Ross Sea (i.e., RIS), and also one order of magnitude lower than in Wilkes Land, East Antarctica (Valletta et al., 2018), and half that of the LIS region (Fig. 2).

^{10}Be LCOs show the greatest variations in the ERS and CRS, but little variation in the WRS (Figs. 3 and 4c). A maximum ^{10}Be concentration (~3×10^9 atoms/g) has been reported for the outer ERS, but the homogeneous ^{10}Be across the Ross Sea and hypothetical concentrations of the Antarctic oceans (~9×10^7 atoms/g) that are two orders of magnitude less than this maximum suggest that other processes are involved (Field et al., 2006; Heikkilä, 2007; Willenbring and von Blanckenburg, 2010a; Yokoyama et al., 2016; Valletta et al., 2018). Our low ^{10}Be concentrations for the WRS (~5×10^8 atoms/g) are still higher than the hypothetical concentrations, but show the least deviation amongst reported data for the whole Ross Sea. Therefore, it can be inferred that the WRS has the most stable depositional conditions, with little contaminations of ^{10}Be and ^{9}Be by reworking. This is consistent with the small LCO of old carbon materials in the WRS, whereas CRS cores are highly contaminated by old carbon (Fig. 4e; Prothro et al., 2020). The small ^{9}Be LCO, limited advection or reworking of surface sediments, and low melt-water flux in the WRS suggest it has the most stable depositional conditions in the various Ross Sea sectors.

^{10}Be concentrations in the CRS and ERS tend to increase toward the outer shelf, which is unlike the WRS where the concentrations decrease toward the outer shelf and exhibit little variability. In the case of the CRS, it has been proposed that the lower ^{10}Be concentrations are due to higher annual sea ice concentrations (Sjunneskog et al., 2007). The similarly lower ^{10}Be concentration pattern in the ERS, which is near the RIS edge, is due to the sub-ice conditions (Yokoyama et al., 2016). In both cases, sea ice extent would have a negative correlation with ^{10}Be deposition, as it acts as a sea surface barrier. However, both the CRS and ERS have positive correlations between the observed sea ice concentration and ^{10}Be deposition (Fetterer et al., 2017; Figs. 4f and 5), which are also related to changes in sea ice extent (Figs. 4 and 5). The RIS Polynya (RISP) and Terra Nova Bay Polynya (TNBP) remove weakened sea ice during summer from these to other regions, which results in early opening (i.e., ice-free conditions) of the mid-WRS and CRS (Sedwick et al., 2011; Fig. 4f). The RIS front and Terra Nova Bay only receive ^{10}Be from in situ sea ice melting and direct fallout during the summer. Sea ice in the outer CRS and ERS becomes highly concentrated by the two polynya and delivers substantial amounts of ^{10}Be to the seafloor when it fully melts. As such, high ^{10}Be concentrations occur near the sea ice "cemetery" in the outer Ross Sea. This is consistent with the ^{10}Be export or transportation which are controlled by sea ice extent changes and ocean currents in Arctic and Antarctic Oceans (Eisenhauer et al., 1994; Kumar et al., 1995; Frank et al., 2000, 2008). The only difference is that the sea ice extent and its cemetery location is more affected by the Polynya wind rather than the ocean current in the bay-shaped Ross Sea. Our extraordinary elevated ^{10}Be concentration at the location of LC47 (Southern Ocean; Fig. 2) also corresponds well with the location of the sea ice cemetery.

The WRS coastal cores tend to have a negative correlation between ^{10}Be and sea ice concentration ($R^2 = 0.67$ and $\rho = -0.82$), but the limited variations in the Be data preclude a robust evaluation of this correlation (Fig. 5). Furthermore, the very low ^{9}Be concentrations in the WRS were due to a different depositional environment. The ^{10}Be/^{9}Be ratios exhibit a positive correlation with sea ice concentration (Figs. 4d and 5). Although the correlation coefficient is very low ($R^2 = 0.01$ and $\rho = 0.11$), due to the limited variations of ^{10}Be in the WRS, the higher and lower sea ice concentrations and ^{10}Be/^{9}Be ratios of the WRS and CRS, respectively, are clearly evident on a scatter plot (Fig. 5). ^{10}Be/^{9}Be ratios in the CRS (R2 = 0.52 and $\rho = 0.72$) and the entire Ross Sea (R2 = 0.57 and $\rho = 0.75$) have a better positive correlation with sea ice concentration as compared with the ^{10}Be concentrations.

The higher ^{10}Be concentrations in the ERS and higher ^{10}Be/^{9}Be ratios in the WRS correspond to higher summer mean sea ice concentrations and extent changes, which highlights the different effects of sea ice and the ice shelf (Figs. 4 and 5). Our findings are consistent with the larger diatom blooms and higher iron and nitrate supply near the WRS coast and outer ERS that is the result of summer sea ice loss (Cunningham and Leventer, 1998; McGillicuddy Jr. et al., 2015). The ice shelf acts as a permanent barrier to meteoric Be isotope fallout during glacial periods or in glaciated regions, whereas sea ice is only a seasonal barrier and diffuser during the warm melting season, especially in the sea ice "cemetery" region. The graphical comparison with the kernel interpolated isotope records and correlation analyses show that seasonal sea ice persistence is the major control on the LCOs of authigenic ^{10}Be concentrations and ^{10}Be/^{9}Be ratios (Figs. 4 and 5). Scavenging and secondary reworking of the marine sediment may have a minor influence on the seafloor Be data, but our measured and compiled data for different glacial and open marine settings show that the LCOs for Be are mainly controlled by sea surface cryospheric conditions.

6. CONCLUSIONS

Significant differences in seafloor sedimentation conditions are recorded by Be isotopes in sub-ice shelf (high ^{9}Be and low

https://doi.org/10.1007/s12303-022-0003-4

^{10}Be), recently collapsed ice shelf (high ^{9}Be and ^{10}Be), and open marine settings (a complex spatial distribution of Be isotopes). Although the same open marine conditions may have existed for thousands of years, Be isotope concentrations and ^{10}Be/^{9}Be ratios have regional variations due to LCOs.

The WRS has the lowest ^{10}Be and ^{9}Be concentrations as compared with the CRS and ERS. The low ^{9}Be concentrations near the WRS coast are due to its distance from the large-scale RIS and proximity to small-scale, localized, Victoria Land outlet glaciers. The low ^{10}Be concentrations are more similar to the hypothetically calculated results as compared with other areas of the Ross Sea, which suggests that the WRS coastal region has the most stable sedimentation conditions in the Ross Sea. However, the WRS seafloor has higher sediment ^{10}Be/^{9}Be ratios, when the low ^{9}Be concentrations are taken into account. The higher ^{10}Be concentrations in the ERS and higher ^{10}Be/^{9}Be ratios in the WRS correspond to higher summer mean sea ice concentration and changes, which highlights the different effects of sea ice and the ice shelf on the Be systematics.

The RIS acts as a barrier to meteoric ^{10}Be fallout during glacial periods or on glaciated regions, while ^{9}Be is supplied in glacier-proximal regions. The different glacial settings result in variable ^{10}Be/^{9}Be ratios of seafloor sediment, with high ratios in open marine settings and low ratios on recently collapsed or sub-ice shelf areas. Sea ice also acts as a potential barrier to meteoric ^{10}Be fallout, but is a two-sided concentrated diffuser during warm melting seasons, particularly in the sea ice "cemetery". Further Be isotope studies could be used to infer changes in the sedimentary environment and past environmental conditions related to climatic and oceanic current changes around Antarctica.

ACKNOWLEDGMENTS

This research was supported by Korea Polar Research Institute (PE21090).

REFERENCES

Beer, J., McCracken, K., and von Steiger, R., 2012, Cosmogenic radionuclides: theory and applications in the terrestrial and space environments. Springer, Berlin, 428 p. https://doi.org/10.1007/978-3-642-14651-0

Bourlès, D., Klinkhammer, G., Campbell, A.C., Measures, C.I., Brown, E.T., and Edmond, J.J., 1989, Beryllium in marine pore waters: geochemical and geochronological implications. Nature, 341, 731–733. https://doi.org/10.1038/341731a0

Brown, E.T., Edmond, J.M., Raisbeck, G.M., Bourles, D., Yiou, F., and Measures, C.I., 1992a, Beryllium isotope geochemistry in tropical river basins. Geochimica et Cosmochimica Acta, 56, 1607–1624. https://doi.org/10.1016/0016-7037(92)90228-B

Brown, E.T., Measures, C.I., Edmond, J.M., Bourles, D.L., Raisbeck, G.M., and Yiou, F., 1992b, Continental inputs of Beryllium to the oceans. Earth and Planetary Science Letters, 114, 101–111. https://doi.org/10.1016/0012-821X(92)90154-N

Cunningham, W.L. and Leventer, A., 1998, Diatom assemblages in surface sediments of the Ross Sea: relationship to present oceanographic conditions. Antarctic Science, 10, 134–146. https://doi.org/10.1017/S0954102098000182

Diekmann, B. and Kuhn, G., 1999, Provenance and dispersal of glacial-marine surface sediments in the Weddell Sea and adjoining areas, Antarctica: ice-rafting versus current transport. Marine Geology, 158, 209–231. https://doi.org/10.1016/S0025-3227(98)00165-0

Eisenhauer, A., Spielhagen, R.F., Frank, M., Hentzschel, G., Mangini, A., and Kubik, P.W., 1994, ^{10}Be records of sediment cores from high northern latitudes: implications for environmental and climatic changes. Earth and Planetary Science Letters, 124, 171–184. https://doi.org/10.1016/0012-821X(94)00069-7

Fetterer, F.K., Knowles, W.N., Meier, M., Savoie, A.K., and Windnagel, H., 2017, Sea ice index, version 3. National Snow and Ice Data Center (NSIDC), Boulder, USA. https://nsidc.org/data/G02135/versions/3

Field, C.V., Schmidt, G.A., Koch, D., and Salyk, C., 2006, Modeling production and climate-related impacts on ^{10}Be concentration in ice cores. Journal of Geophysical Research, 111, D15107. https://doi.org/10.1029/2005JD006410

Frank, M., Backman, J., Jakobsson, M., Moran, K., O'Regan, M., King, J., Haley, B.A., Kubik, P.W., and Garbe-Schönberg, D., 2008, Beryllium isotopes in central Arctic Ocean sediments over the past 12.3 million years: stratigraphic and paleoclimatic implications. Paleoceanography, 23, PA1S02. https://doi.org/10.1029/2007PA001478

Frank, M., Eisenhauer, A., Bonn, W.J., Walter, P., Grobe, H., Kubik, P.W., Dittrich-Hannen, B., and Mangini, A., 1995, Sediment redistribution versus paleoproductivity change: Weddell Sea margin sediment stratigraphy and biogenic particle flux of the last 250,000 years deduced from 230Thex, ^{10}Be and biogenic barium profiles. Earth and Planetary Science Letters, 136, 559–573. https://doi.org/10.1016/0012-821X(95)00161-5

Frank, M., Gersonde, R., van der Loeff, M.R., Bohrmann, G., Nürnberg, C.C., Kubik, P.W., Suter, M., and Mangini, A., 2000, Similar glacial and interglacial export bioproductivity in the Atlantic sector of the Southern Ocean: multiproxy evidence and implications for glacial atmospheric CO_2. Paleoceanography, 15, 642–658. https://doi.org/10.1029/2000PA000497

Frank, M., Porcelli, D., Andersson, P., Baskaran, M., Björk, G., Kubik, P.W., Hattendorf, B., and Guenther, D., 2009, The dissolved Beryllium isotope composition of the Arctic Ocean. Geochimica et Cosmochimica Acta, 73, 6114–6133. https://doi.org/10.1016/j.gca.2009.07.010

Frank, M., van der Loeff, M.R., Kubik, P.W., and Mangini, A., 2002, Quasi-conservative behaviour of ^{10}Be in deep waters of the Weddell Sea and the Atlantic sector of the Antarctic Circumpolar Current. Earth and Planetary Science Letters, 201, 171–186. https://doi.org/10.1016/S0012-821X(02)00688-X

Gerringa, L.J., Alderkamp, A.C., Van Dijken, G., Laan, P., Middag, R., and Arrigo, K.R., 2020, Dissolved trace metals in the Ross Sea. Frontiers in Marine Science, 7, 874. https://doi.org/10.3389/fmars.2020.577098

Heikkilä, U., 2007, Modeling of the atmospheric transport of the cosmogenic radionuclides ^{10}Be and ^{7}Be using the ECHAM5-HAM General Circulation Model. Ph.D. Thesis. ETH-Zürich, Zürich, 148 p. https://doi.org/10.3929/ethz-a-005560259

Hillenbrand, C.D., Smith, J.A., Kuhn, G., Esper, O., Gersonde, R., Larter, R.D., Maher, B., Moreton, S.G., Shimmield, T.M., and Korte, M., 2010, Age assignment of a diatomaceous ooze deposited in the western Amundsen Sea Embayment after the Last Glacial Maximum. Journal of Quaternary Science, 25, 280–295. https://doi.org/10.1002/jqs.1308

Jeong, A., Lee, J.I., Seong, Y.B., Balco, G., Yoo, K.C., Yoon, H.I., Domack, E., Rhee, H.H., and Yu, B.Y., 2018, Late Quaternary deglacial history across the Larsen B embayment, Antarctica. Quaternary Science Reviews, 189, 134–148. https://doi.org/10.1016/j.quascirev.2018.04.011

Jung, J., Yoo, K.C., Rosenheim, B.E., Conway, T.M., Lee, J.I., Yoon, H.I., Hwang, C.Y., Yang, K., Subt, C., and Kim, J., 2019, Microbial Fe(III) reduction as a potential iron source from Holocene sediments beneath Larsen Ice Shelf. Nature Communications, 10, 5786. https://doi.org/10.1038/s41467-019-13741-x

Kumar, N., Anderson, R.F., Mortlock, R.A., Froelich, P.N., Kubik, P., Dittrich-Hannen, B., and Suter, M., 1995, Increased biological productivity and export production in the glacial Southern Ocean. Nature, 378, 675–680. https://doi.org/10.1038/378675a0

Lowry, D.P., Golledge, N.R., Bertler, N.A.N., Jones, R.S., McKay, R., and Stutz, J., 2020, Geologic controls on ice sheet sensitivity to deglacial climate forcing in the Ross Embayment, Antarctica. Quaternary Science Advances, 1, 100002. https://doi.org/10.1016/j.qsa.2020.100002

McGillicuddy Jr., D.J., Sedwick, P.N., Dinniman, M.S., Arrigo, K.R., Bibby, T.S., Greenan, B.J.W., Hofmann, E.E., Klinck, J.M., Smith Jr., W.O., Mack, S.L., Marsay, C.M., Sohst, B.M., and Van Dijken, G.L., 2015, Iron supply and demand in an Antarctic shelf ecosystem. Geophysical Research Letters, 42, 8088–8097. https://doi.org/10.1002/2015GL065727

Mühlenstädt, T. and Kuhnt, S., 2011, Kernel interpolation. Computational Statistics & Data Analysis, 55, 2962–2974. https://doi.org/10.1016/j.csda.2011.05.001

Nishiizumi, K., Imamura, M., Caffee, M.W., Southon, J.R., Finkel, R.C., and McAninch, J., 2007, Absolute calibration of ^{10}Be AMS standards. Nuclear Instruments and Methods in Physics Research Section B: Beam Interactions with Materials and Atoms, 258, 403–413. https://doi.org/10.1016/j.nimb.2007.01.297

Prothro, L.O., Majewski, W., Yokoyama, Y., Simkins, L.M., Anderson, J.B., Yamane, M., Miyari, Y., and Ohkouchi, N., 2020, Timing and pathways of East Antarctic Ice Sheet retreat. Quaternary Science Reviews, 230, 106166. https://doi.org/10.1016/j.quascirev.2020.106166

Thor, R. and Zutshi, P.K., 1958, Annual deposition of cosmic ray produced Be^{7} at equatorial latitudes. Tellus, 10, 99–103. https://doi.org/10.3402/tellusa.v10i1.9214

Scherer, R.P., Aldahan, A., Tulaczyk, S., Possnert, G., Engelhardt, H., and Kamb, B., 1998, Pleistocene collapse of the West Antarctic ice sheet. Science, 281, 82–85. https://doi.org/10.1126/science.281.5373.82

Sedwick, P.N., Marsay, C.M., Sohst, B.M., Aguilar-Islas, A.M., Lohan, M.C., Long, M.C., Arrigo, K.R., Dunbar, R.B., Saito, M.A., Smith, W.O., and DiTullio, G.R., 2011, Early season depletion of dissolved iron in the Ross Sea polynya: implications for iron dynamics on the Antarctic continental shelf. Journal of Geophysical Research: Oceans, 116, C12019. https://doi.org/10.1029/2010JC006553

Shepherd, A., Wingham, D., Payne, T., and Skvarca, P., 2003, Larsen ice shelf has progressively thinned. Science, 302, 856–859.

Simon, Q., Thouveny, N., Bourles, D.L., Nuttin, L., Hillaire-Marcel, C., and St-Onge, G., 2016, Authigenic ^{10}Be/^{9}Be ratios and ^{10}Be-fluxes (230Thxs-normalized) in central Baffin Bay sediments during the last glacial cycle: paleoenvironmental implications. Quaternary Science Reviews, 140, 142–162. https://doi.org/10.1126/science.1089768

Sjunneskog, C., Scherer, R., Aldahan, A., and Possnert, G., 2007, ^{10}Be in glacial marine sediment of the Ross Sea, Antarctica, a potential tracer of depositional environment and sediment chronology. Nuclear Instruments and Methods in Physics Research Section B: Beam Interactions with Materials and Atoms, 259, 576–583. https://doi.org/10.1016/j.nimb.2007.01.203

Stone, J., 1998, A rapid fusion method for separation of beryllium-10 from soils and silicates. Geochemica et Cosmochimica Acta, 62, 555–561. https://doi.org/10.1016/S0016-7037(97)00340-2

Valletta, R.D., Willenbring, J.K., Passchier, S., and Elmi, C., 2018, ^{10}Be/^{9}Be ratios reflect Antarctic Ice Sheet freshwater discharge during Pliocene warming. Paleoceanography and Paleoclimatology, 33, 934–944. https://doi.org/10.1029/2017PA003283

von Blanckenburg, F., O'Nions, R.K., Belshaw, N.S., Gibb, A., and Hein, J.R., 1996, Global distribution of Beryllium isotopes in deep ocean water as derived from Fe-Mn crusts. Earth and Planetary Science Letters, 141, 213–226. https://doi.org/10.1016/0012-821X(96)00059-3

von Blanckenburg, F. and Bouchez, J., 2014, River fluxes to the sea from the ocean's ^{10}Be/^{9}Be ratio. Earth and Planetary Science Letters, 387, 34–43. https://doi.org/10.1016/j.epsl.2013.11.004

von Blanckenburg, F., Bouchez, J., Ibarra, D.E., and Maher, K., 2015, Stable runoff and weathering fluxes into the oceans over Quaternary climate cycles. Nature Geoscience, 8, 538–542. https://doi.org/10.1038/ngeo2452

Wang, S., Bailey, D., Lindsay, K., Moore, J.K., and Holland, M., 2014, Impact of sea ice on the marine iron cycle and phytoplankton productivity. Biogeosciences, 11, 4713–4731. https://doi.org/10.5194/bg-11-4713-2014

White, D.A., Fink, D., Post, A.L., Simon, K., Galton-Fenzi, B., Foster, S., Fujioka, T., Jeromson, M.R., Blaxell, M., and Yokoyama, Y., 2019, Beryllium isotope signatures of ice shelves and sub-ice shelf circulation. Earth and Planetary Science Letters, 505, 86–95. https://doi.org/10.1016/j.epsl.2018.10.004

Willenbring, J.K. and von Blanckenburg, F., 2010, Meteoric cosmogenic Beryllium-10 adsorbed to river sediment and soil: applications for Earth-surface dynamics. Earth-Science Reviews, 98, 105–122. https://doi.org/10.1016/j.earscirev.2009.10.008

Yokoyama, Y., Anderson, J.B., Yamane, M., Simkins, L.M., Miyairi, Y., Yamazaki, T., Koizumi, M., Suga, H., Kusahara, K., Prothro, L., Hasumi, H., Southon, J.R., and Ohkouchi, N., 2016, Widespread collapse of the Ross Ice Shelf during the late Holocene. Proceedings of the National Academy of Sciences of the United States of America, 113, 2354–2359. https://doi.org/10.1073/pnas.1516908113